FURTHER RESULTS ON THE OPERATION OF HIGH-ACCURACY DRIFT CHAMBERS

A. BRESKIN*, G. CHARPAK, B. GABIOUD**, F. SAULI and N. TRAUTNER*

CERN, Geneva, Switzerland

W. DUINKER

Utrecht State University, Holland

and

G. SCHULTZ

Centre de Recherches Nucléaires, Université L. Pasteur, Strasbourg, France

Optimization of the working parameters in the drift chambers with adjustable electric fields permits stable operation and high accuracies. Full saturation of the drift velocity leads to remarkable improvements, namely a very linear space–time correlation for perpendicular tracks, and simple geometrical distortion of linearity for inclined tracks. The same results can be obtained when properly tilting the electric field equipotentials in a wide range of external magnetic fields. This simple behaviour should allow a practical use, even for large systems, of the intrinsic high accuracy of the drift chambers (100–200 μm). They appear then as a very promising high-resolution fast detector for high-energy particle physics.

1. Introduction

Multiwire proportional chambers (MWPC) have been introduced at CERN several years ago and fulfill the growing requirements of selective and fast data collection in high-energy physics detectors[1]. Since then, a lot of effort has been devoted to their development[2]), and nowadays detectors using large sets of MWPC exist with as much as 65 000 wires in a single experimental set-up[3]). Although very attractive for their self-triggered operation and good time and multi-particle resolution, the present-day MWPC are rather expensive, mainly due to the large amount of electronics needed: in the classical scheme an amplifier, discriminator, delay, and gated memory on each wire. Moreover, the accuracy of a conventional MWPC is limited by the wire spacing, which for large-surface detectors cannot be safely reduced below 2 mm.

With the nowadays growing accelerator energies, and since there are practical limits to the bending power of magnetic spectrometers, higher accuracies are desirable to achieve good momentum resolution. Also, at very high energies, the multiple Coulomb scattering is not any longer an intrinsic limitation to the desired space accuracy.

Already in the early stage of development of MWPC

it was noticed that a knowledge of the time of collection, or time of drift, of the primary electrons within the chamber could provide additional information on the position of the detected ionizing particle[4]). Special chambers, consisting essentially of a long and thin detection space with uniform electric field (the drift space), and of a thin amplifying anode wire at one end were constructed and even used in experiments[5,6]). Although providing rather accurate position measurement with simple electronics, this design is seriously limited in the flux of particles that can be unambiguously detected when large sensitive volumes are aimed at.

An alternative approach has been to maintain the structure of a conventional MWPC, increasing, however, the wire spacing to reduce the number of channels and measuring the time of drift on each wire[7-9]). The right–left ambiguity, intrinsic to such a scheme, can be removed either by track reconstruction in a set of staggered chambers, or by replacing each anode wire by a triplet of wires, two thin anodes separated by a screening electrode[7]). A proper voltage gradient in the triplet also minimizes the electrostatic forces. Large and very large set-ups using this design have been constructed and operated. A strong limitation of the methods lies, however, in the fact that, to avoid in the chamber design low-field pockets that would delay or trap primary electrons producing localized inefficiencies, the gap dimension should be maintained about equal to the wire spacing. For large

---

* Present address: Weizmann Institute of Science, Rehovot, Israel.
** Present address: Institut de Physique, Université de Lausanne, Switzerland.
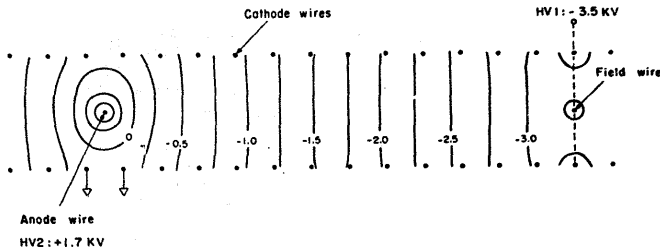
A. BRESKIN et al.

Fig. 1. Equipotentials in half a cell of the adjustable electric field drift chamber. The cathode-wire spacing is 2 mm, the distance between cathodes 6 mm and the cell length (field wire to field wire) 50 mm. In the centre is placed the anode wire with 20 μm diameter connected to a positive potential +HV2. The potential is uniformly distributed on the cathode wires, from zero (in front of the anode) to the maximum value −HV1.

wire spacings, therefore, the chambers should be rather thick and the average density of detection planes on a particle trajectory is low. This is a serious drawback, particularly for vertex detectors operating in magnetic fields, where a large number of coordinates per track must be measured on a limited length to allow reconstruction of low-momentum particles. Also, thick chambers are more sensitive to X- and γ-ray backgrounds.

The problem can be overcome by constructing an Adjustable Electric Field Drift Chamber (AFDC), where a suitable voltage gradient applied to the cathode wires permits long drift spaces with high electric field even at small gaps[10]). In this paper we describe further results of a systematic study of the AFDC, operating in various conditions and inside strong magnetic fields, with appreciable improvements on the results quoted in ref. 10.

2. Basic operation of the adjustable-electric-field drift chambers

As has been shown in ref. 10, it is possible to obtain long drift spaces with high electric fields in a modified MWPC structure for any wire spacing. The principle of construction is repeated in fig. 1, which represents a cross cut of part of a drift cell in the AFDC. The cathode planes are made by two sets of parallel, 100 μm diameter, wires, 2 mm apart; the distance between the cathode planes is 6 mm. Accessory electrodes, the field wires, 50 mm apart, are mounted between the cathode planes to better delimitate the drift space of one cell. An increasingly negative potential applied to the cathode wires, symmetric around the centre of the cell, creates a

strong and rather uniform electric field directed towards the central anode wire.

The primary electrons produced in the gas by a charged particle move then towards the central thin anode wire (20 μm diameter) and are here amplified and detected. The gain of the cell can be adjusted by varying the anodic (positive) potential; in figs 1 and 2 the equipotentials and the field in the central plane of the cell are shown for a typical operation at $HV1 = -3.5$ kV and $HV2 = +1.7$ kV. Operating the AFDC with inde-
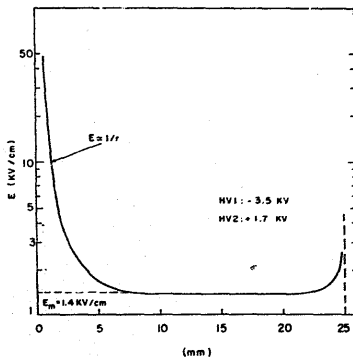

Fig. 2. Electric field, in kV/cm, as measured in a central plane of the chamber, $s = 0$ being the position of the anode wire and $s = 25$ mm the position of the field wire. In no point of the chamber is the field lower than $E_m = 1.4$ kV/cm.

pendent drift and anodic potentials has permitted a considerable number of improvements, as compared with the original design[10] where the anode wire was grounded, since the two parameters (drift and anodic fields) could easily be adapted to other conditions, like the gas composition and the magnetic fields, for optimum performance.

It was already shown in the previous work that accuracies of the order and even below 100 μm could be obtained in the AFDC by measuring the time of drift of the primary electrons in the cell, referred to a zero time provided by external scintillation counters. We have since then been working to understand better the properties of the AFDC in view of possible large-scale applications; in particular, we have measured the modification of the drift velocity and direction induced by reasonable variations of the electric fields, of temperature, and of gas composition. Also, a large effort was devoted to obtaining proper operation in strong magnetic fields, and the limits within which we believe the good intrinsic accuracy can be maintained are discussed. In the following text, section 3 illustrates the work on the optimization of the gas composition and chamber operation. In section 4 we describe the results obtained in operating AFDC of small and medium size without magnetic fields, and in section 5 the operation in weak and strong magnetic fields. The last sections are devoted to further possible developments of the AFDC.

3. Methods of measurement and optimization of the operational parameters

We have used different chambers and methods for the systematic study of the drift properties in gases. Here we would like to describe the way the most relevant parameters have been measured.

3.1. MEASUREMENT OF THE DRIFT VELOCITY AS A FUNCTION OF THE ELECTRIC FIELD

A special chamber, similar in design to those described in refs. 4–6, has been built. It consists of a drift region, where a uniform, externally controlled electric field can be applied, and a thin anode wire at one end to collect and amplify the drifting charges. A collimated radioactive β source can be displaced along the drift region, and a scintillation counter provides the time-zero reference (fig. 3). The drift time is then measured, and the drift velocity deduced from the time difference between two known positions of the source. Varying the applied potential, the drift velocity as a function of the electric field can be measured for different gas mixtures.

The particular construction of the chamber makes it possible also to tilt the equipotentials in the drift region, so as to permit the operation in strong magnetic fields[10] (see also section 5). The systematic research on drift velocities and angles in magnetic fields will be discussed in a separate paper[11]. Here we would like to stress that our main concern from the very beginning has been to find a gas mixture in which the drift velocity is independent of the electric field, above a critical value E_c. There are many reasons for that. First, having a saturated drift velocity everywhere in a chamber leads to perfect linearity in the space–time relationship, or to simple geometrical deformations of linearity as in the case of inclined tracks (see the next section). This is certainly very useful in order to reduce the complexity of data handling. But also, and we think this is even more important, a saturated operation makes the chamber response virtually independent of local imperfections and mechanical tolerances in the construction of the cathode planes. In fact, in our design of the AFDC the electric field is nowhere smaller than a minimum value E_m (see fig. 2) and we could easily operate with $E_m \gg E_c$. Furthermore, it appeared that a
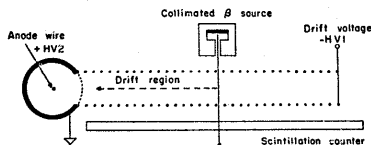

Fig. 3. Special chamber used for the measurement of the drift velocity. A uniform-field drift region is followed by a proportional counter to detect the drift time; the field strength can be varied modifying the value of $-HV1$.
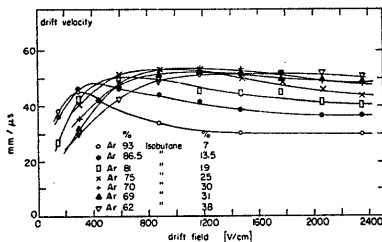

Fig. 4. Measured drift velocities for different argon–isobutane mixtures, as a function of the electric field, showing the saturation effect.

saturated operation minimizes the changes of the drift velocity with temperature, pressure, and gas composition. Many gas mixtures are known to produce saturation. For convenience, we have mainly used argon–isobutane; fig. 4 shows the measured drift velocity w as a function of E for different percentages of isobutane in argon (all measurements at atmospheric pressure). It can be seen that for a mixture corresponding to about 31% C_4H_{10}, the drift velocity is constant above $E_c \simeq 1000$ V/cm and up to the maximum value we could attain, about 2.4 kV/cm *. Looking back to the design of a real AFDC, fig. 1, it is clear that this range covers most of the chamber with the exception of the region close to the anode wire. Here, the field increases by several orders of magnitude to reach the 10^5 V/cm necessary to obtain gas multiplication. Although we could not directly measure the drift velocity at such fields in the previously described chamber, the perfect linearity in the space–time relationship verified close to the anode in the AFDC (see next section) confirms that saturation extends to the highest values of the electric field, up to the point where avalanche multiplication takes place.

Consequently, in all the following measurements the gas mixture was maintained constant at the quoted value, with, however, the addition of a small quantity of methylal $\{(OCH_3)_2CH_2\}$ as a quencher to avoid polymerization of isobutane at high particle fluxes[13]. We have verified that the addition does not modify the behaviour of the drift velocity; the finally adopted gas mixture has 67.2% argon, 30.3% isobutane and 2.5% methylal.

By varying the gas composition and temperature around the central value, we could then easily verify the sensitivity of the drift velocity at saturation, w_s, in the environment. The following variations have been measured:

i) temperature dependence: $\Delta w_s/w_s = 3 \times 10^{-4}/{}^\circ C$;

ii) gas composition dependence: $\Delta w_s/w_s = 1.2 \times 10^{-3}/$ % isobutane;

iii) pressure dependence: zero for small variations around the atmospheric pressure.

For the operation of high accuracy AFDC a stability equivalent to 100 μm over the maximum drift space seems sufficient, at least in the framework of the present study; for 50 mm wire spacing, this corresponds to a maximum $\Delta w_s/w_s$ of 4×10^{-3}. We could then tolerate, without corrections to the data, over-all temperature variations of about 14 °C; the gas mixture had to be

---

* A discussion on the theory governing the drift velocities in mixtures of gases has recently been put forward by Palladino and Sadoulet[12]).

---

stabilized to ±1.5% in the isobutane content. It is, of course, always possible, in a real experiment, to monitor the actual value of the drift velocity in a special set-up similar to the one described for these measurements. The maximum drift time in a chamber that can be monitored continuously, provides also a good and simple check of the drift-velocity stability.

It should be noticed that the drift velocity in the non-saturated region, below E_c, is much more dependent on the external parameters. Around $E = 600$ V/cm, we have measured a variation of w with temperature and gas about four times larger than the quoted values at saturation. Obviously, in this region the drift velocity is also strongly dependent on the electric field: we found $\Delta w/w = 0.05$ for an 8% change in the applied voltage. This means that to maintain the quoted 100 μm stability over 25 mm of drift, a 0.6% tolerance on the electric field value in the drift region of the chamber would be demanded. This is, of course, the strongest argument in favour of the saturated mode of operation. The only way to detect local variations of E (and therefore of w) would be the integral-spectra method, to be discussed next; we are not sure, however, whether it can be precise enough.

The value of the drift velocity at saturation, about 5 cm/μs, is also rather convenient; to keep the 100 μm accuracy level, a 2 ns time-digitizing electronics is demanded, and this seems reasonable for present-day digital integrated-circuit technology[14–16]). Faster gases, although they are useful in reducing the memory time of a chamber, require accuracies difficult to reach using digital techniques, and analogue time-measuring techniques [like the time stretchers[17])] may have to be used.

It also appeared rather difficult to design simple amplifiers and triggers to detect the signals on the anode wires with an electronic time slewing below 2–3 ns for the wide range of input pulses; the higher the drift velocity, the larger of course the effect of the electronics jitters on the final accuracy.

3.2. The integral-time-spectra method to obtain the drift velocity

We have used a simple method to explore rapidly the behaviour of the drift velocity[9]). The drift chamber under study is exposed to a β source, or, better, installed in a high-energy charged-particle beam, and as before a scintillation counter provides the time reference. On a multichannel analyser we record the distribution of events per time bin, dN/dt, in the interval from zero to the maximum drift time (fig. 5).

One can write:

$$\frac{dN}{dt} = \frac{dN}{ds}\frac{ds}{dt} = \frac{dN}{ds} w(t), \qquad (1)$$

where s is the coordinate along the drift direction in the chamber. Hence, if the beam has a uniform distribution in space, the time distribution dN/dt is proportional to the drift velocity $w(t)$, and its integral reproduces the $s = s(t)$ relationship. The method is inaccurate for two reasons. First, it is very hard to guarantee uniformity of a beam over the rather large acceptance of a drift chamber, at a level we need (four parts in a thousand). Secondly, the absolute calibration of the space–time scales is provided by the assumption that the maximum recorded drift time T_0 corresponds to the geometrical maximum drift space S_0. This is not true, for example, in the case of inclined tracks (where the acceptance is wider at the separation between two adjacent cells of an AFDC, see the next section) and is in any case wrong if there are localized inefficiencies. We have used this method, therefore, only for a quick survey of the overall behaviour of chambers in different conditions.

3.3. PRECISE MECHANICAL SCANNING TO OBTAIN $s = s(t)$

The method, despite its inconvenience, has been found to be the only one that effectively guarantees the results to the required degree of precision. The chamber under study is mounted between two collimation chambers (DC1 and DC3 in fig. 6), and can be displaced horizontally by a micrometric movement. When the system is mounted on a beam, a narrow coincidence between DC1, DC3, and a scintillation counter can select events at a given time distance from the anode wire of the collimators. A coincidence close to the minimum of the drift-time distribution then electronically selects a thin pencil beam in the centre of the system. We could experimentally achieve stable operation with selected beams as narrow as 50 μm fwhm (corresponding to 1 ns coincidence width). Displacing the test chamber along the s direction, and recording its time distribution gated by the collimators, we could then precisely obtain the space–time relationship. The method works for any angle of incidence in the central chamber and in magnetic fields; the origins of space and time coordinates are deduced from the measurement itself (see fig. 6). Setting the coincidence in the collimators at a time different from zero, due to the right–left symmetry in the drift chambers, two pencil beams are selected, thus doubling the measured points for each position during the scanning. In this case, however, one has to rely on the stability of operation (constant drift velocity) of the collimating chambers, while using a selection close to the minimum time the effect of instabilities is minimized.

3.4. MEASUREMENT OF THE SPACE ACCURACY OF DRIFT CHAMBERS
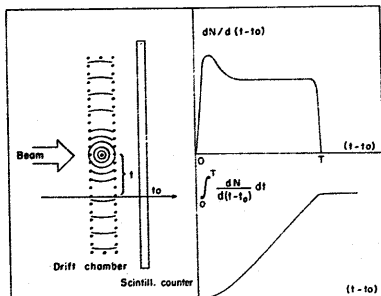
With the same set-up as in fig. 6, but aligning the

Fig. 5. The integral-spectrum method for a rough check of the drift velocity. A plot of the time distribution given by the chamber in a uniform beam provides information on the space–time relationship.
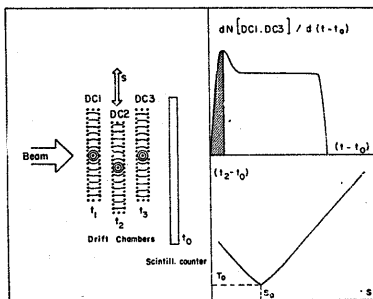

Fig. 6. The precise mechanical scanning method to deduce the space–time relationship. The two outer chambers are used as a collimator: an electronic coincidence on their time spectrum, near to $t = t_0$, selects a thin pencil beam crossing the chambers close to the anode wires. The chamber under study, DC2 in the figure, is then mechanically displaced recording the time spectra in coincidence with the collimator for each position. A space–time relationship is then obtained as shown.

three (equal) chambers on the beam, the intrinsic accuracy of the drift chambers can be measured. We record for each track the drift times t_1, t_2, t_3 and compute the quantity:

$$\Delta(t_2) = \tfrac{1}{2}(t_1 + t_3) - t_2. \qquad (2)$$

From the distribution of $\Delta(t_2)$ about given values of t_2, we can then deduce its standard deviation σ_Δ and, assuming equal errors and close times of drift in the three chambers, the intrinsic accuracy of each chamber $\sigma(t) = (\tfrac{2}{3})^{\frac{1}{2}}\sigma_\Delta$ as a function of the average time of drift. The method works as well with simple modifications when the chambers are inclined with respect to the beam, and in magnetic fields (for constant beam momentum). To compute the accuracy as a function of the drift space (deduced from the average time and the known drift velocity) we used standard CAMAC time-to-digital converters and a small on-line computer. At the same time auxiliary parameters like efficiency and time distributions could be monitored on a display screen during the run.

We should also mention that for convenience we used for all measurements fast linear preamplifiers* on the chambers followed by standard NIM discriminators. It was possible to monitor also the pulse-height distributions and shapes. Moreover, to guarantee a stable gas mixture for long runs, the gas supply system was maintained at constant temperature ($\pm 2\,^\circ$C) and the ambient temperature was verified so as not to vary by more than the quoted tolerance (about 15 $^\circ$C).
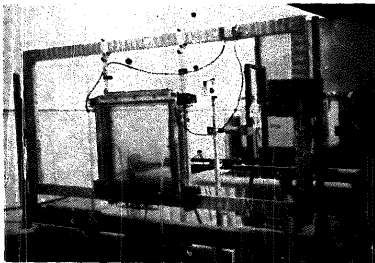
* Designed at CERN by H. Verweij.

Fig. 7. View of a 50×50 cm^2 (useful surface) drift chamber, installed in a test beam for the measurements described. The large chamber has three independent coordinate planes, each with 10 anode wires.

4. Operation of AFDC without external magnetic fields

4.1. PRINCIPLES OF CONSTRUCTION OF A DRIFT CHAMBER

All chambers have been constructed using conventional MWPC techniques (see, for example, ref. 13) requiring however all parts to satisfy a stricter mechanical tolerance in order not to spoil the final accuracy of localization. Double-face printed circuits are glued to surfaced fibre-glass frames and the cathode (or anode) wires are stretched and soldered to them; proper assembly of several frames makes a single or multigap chamber. For small chambers the frames are self-supporting; for chambers exceeding 30×30 cm^2 we had to use instead external aluminium support frames. All our chambers have 6 mm gap (distance between two cathode planes), field wires on the boundary of the cells, and a resistor chain at one end of the cathodic printed-circuit bus to distribute the graded potentials across the chamber. The size of chambers ranges from a few cm^2 (we used these chambers for the measurements in magnetic field) to 50×50 cm^2; a full-scale prototype that will be installed for testing in the CERN superconducting Ω magnet, measuring 220×150 cm^2, is in an advanced stage of construction. The drift cell in the smallest chambers is 48 mm, whereas in all others it is 50 mm. In fig. 7 one can see the largest operational chamber, having a 50×50 cm^2 useful surface and three complete gaps that could be independently operated to study possible interactions of a multigap structure. Most of the measurements in this section refer to the large chamber, while in the next section, devoted to the operation in magnetic fields, only results obtained with the small chambers are presented.

4.2. EFFECT OF INCREASING THE DRIFT VOLTAGE

Using the integral method described in section 3.2, we could easily verify the effect of the drift electric field in the AFDC. A chamber was mounted in the beam perpendicular to it, and the time spectra recorded for several values of the drift voltage, HV1. For each measurement, the value of HV2, the anodic potential, was adjusted so as to obtain the same average pulse height on the beam particles (it should be noticed that a variation of HV1 also affects the gain of the chamber). The result is shown in fig. 8, where the integrals of the time spectra are superimposed; the horizontal scale represents the time of drift, and the vertical the space (maximum 25 mm). The curves, from the lowest up, refer to increasing values of HV1 from -500 to -3500 V in regular steps (the last two curves overlap). The saturation effect is clearly visible at the largest values of the drift potential; the value HV1 $= -3.5$ kV

corresponds to an average field in the drift region of about 1.4 kV/cm, and looking back to fig. 4 one can see that at this value of E the velocity is fully saturated. All measurements in the present work have been realized in this saturated condition.

4.3. PULSE HEIGHT AND EFFICIENCY

We have used the 50×50 cm^2 chamber, fig. 7, installed in a test beam to study pulse height and efficiency for minimum ionizing particles. A typical PH distribution on a wire is shown in fig. 9, as obtained from the output of a current amplifier with 20Ω input impedance; the horizontal scale corresponds to about 10 μA/division. The noise level is rather high, due to poor screening of the chamber in a very noisy environment; a triggering level between 10 and 15 μA was found suitable for proper operation. The efficiency plateau as a function of the anodic potential is shown in fig. 10 for a beam perpendicular to the chamber

(0°, full curve). The drift voltage, HV1, was kept constant and equal to -3.5 kV during the measurement, and the time resolution slightly longer than the expected time, i.e. 500 ns. For particles traversing the chamber at an angle, a small shift of the plateau

Fig. 10. Efficiency versus anodic voltage of a drift chamber. The drift field has been maintained constant. The efficiency has been measured for minimum-ionizing particles, at two angles of incidence (0° means a beam perpendicular to the chamber).

Fig. 8. Space–time relationships obtained with the integral-time-spectrum method, for a beam perpendicular to the drift chamber and as a function of the drift field. The horizontal scale shows the time of drift, with 100 ns/div., and the vertical scale the space of drift, with 5 mm/div. The different curves, from the lowest up, are obtained increasing the drift potential HV1 (see fig. 1) from -0.5 to -3.5 kV, in steps of 500 V; the last two curves overlap. The saturation effect is clearly visible.
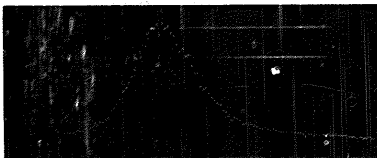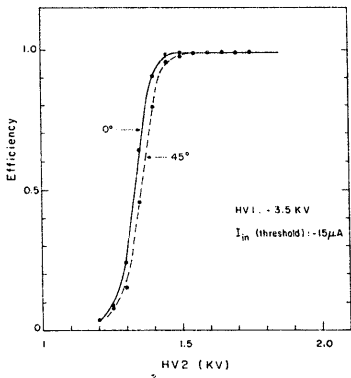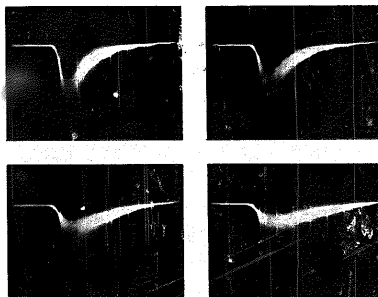

Fig. 9. Pulse-height spectrum of a drift chamber for minimum-ionizing particles, at HV1 = -3.5 kV and HV2 = $+1.7$ kV, as measured with a current amplifier. The horizontal scale is 10 μA/div. In all the following measurements a threshold of detection of about 15 μA has been used.

Fig. 11. Pulse shape as detected on a fast current amplifier (20 Ω input impedance), for several values of the angle of incidence of the beam, upper part: 0° and 20°, lower part: 40° and 60°, respectively. Due to the time spread of the drifting primary electrons, the pulse width increases with the angle. The scales are 20 ns/div. and 10 μA/div. as referred to the input of the amplifier.
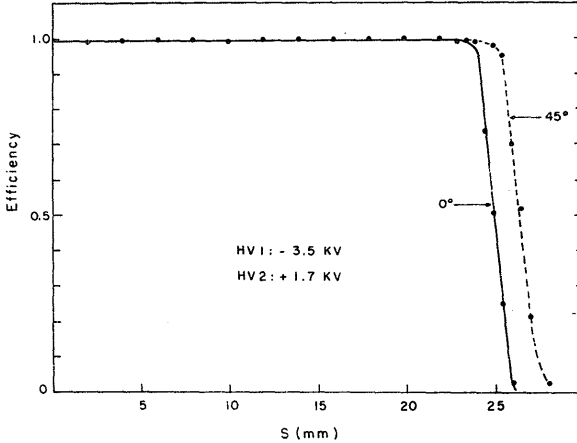
A. BRESKIN et al.

Fig. 12. Efficiency as a function of the drift space, for a chamber having 50 mm wire spacing ($s = 0$ is the position of the anode wire at the centre of the cell). For purely geometrical reasons, the efficiency is wider for inclined tracks.

towards higher voltages was observed, as shown by the broken curve in fig. 10 (at 45°). This is a consequence of the increase, with the angle of incidence, in the time spread of the electrons arriving at the anode that results in a reduced pulse height. In fig. 11 the pulses detected on a wire for increasing angles of incidence are shown; we have observed that the broadening effect tends to disappear at the highest anodic potentials, probably because of a space-charge limitation on the gain (saturation of pulse height) similar to the one observed in the MWPC magic gas[13].

By a manual scanning procedure as described in section 3.3, in coincidence with the small collimator chambers we have measured the efficiency as a function of the position, at constant voltages. The result is shown in fig. 12 for one half of a drift cell (the other half being symmetrically equal). The efficiency is flat and equal to about 99.4% across the cell; notice the increase of the efficient region for inclined tracks, corresponding to the increase in the geometrical cross section (see also fig. 1). The behaviour at the boundary between two cells is better seen in fig. 13, where on a larger scale the efficiency of two neighbouring wires is shown for perpendicular tracks. Owing to the finite width of the collimation (about 0.5 mm fwhm) the transition does

not look as steep as it probably is; no particular structure or loss of efficiency is observed, however, in the region of the field wire.
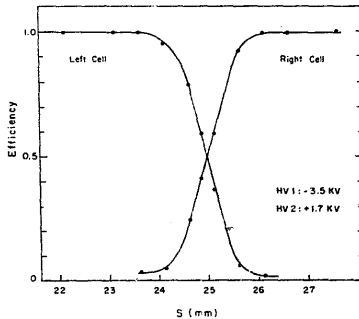

Fig. 13. Expanded view of the efficiency as measured in the transition region between two cells (about the field wire) showing a cross-over at 50%. The moderate steepness of the transition is due to the beam collimation (about 0.5 mm fwhm).

4.4. SPACE–TIME RELATIONSHIP FOR PERPENDICULAR AND INCLINED TRACKS

In fig. 14 (upper part) a time spectrum and its integral are shown for perpendicualr (0°) tracks. As mentioned before, complete saturation of the drift velocity results in a linear response, and this can better be seen in fig. 15 where the space–time correlation deduced with the precise mechanical scanning method is shown. The measured points fit into a straight line having a slope of 19.4 ns per mm. The situation is more complicated when the chamber is inclined with respect to the beam [fig. 14 (lower part)]; two effects appear that perturb the linearity. First, the drift velocity looks increased close to the anode wire; as will appear more clearly below, this is purely a geometrical effect, due to the drift of the primary electrons along a curved trajectory close to the anode. The second effect, more peculiar and unexpected, is a "modulation" of the velocity (in fact of the trajectory) all along the drift space, and with a wavelength corresponding to the cathode-wires spacing
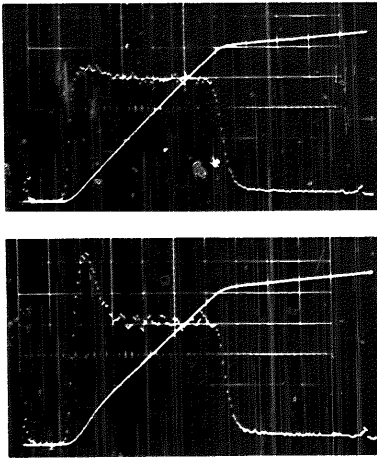

Fig. 14. Upper part: time spectrum and its integral for perpendicular tracks measured as described in fig. 5, showing the effect of saturation. The residual non-linearity is due to the non-uniformity of the beam.
Lower part: the same for a beam at 50° with the normal to the chamber, showing the deviation from linearity due to geometrical reasons (see the text). Horizontal scale: 100 ns/div. in both pictures.

(2 mm). Both effects are better seen in fig. 16, which is an enlarged view of the integral spectrum at 50°. The shape of the spectrum can be explained as follows.

Due to the rather high gain of the chamber and to the low threshold, both necessary to obtain a good time resolution, we were essentially triggering on the first few primary electrons arriving at the wire. For perpendicular tracks, the shortest distance of drift lies in the
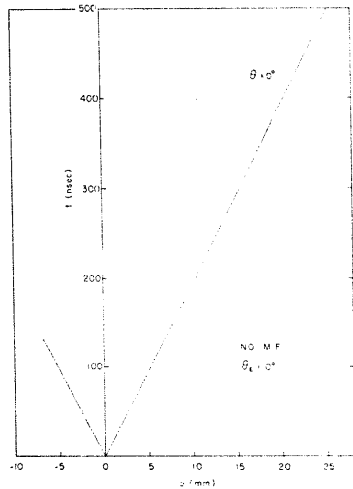

Fig. 15. Space–time relationship as measured for perpendicular tracks with the precise mechanical-scanning method described in fig. 6. Perfect linearity of the correlation is found in all the range.
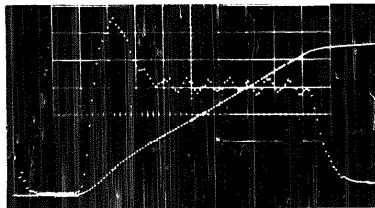

Fig. 16. Expanded view of the integral spectrum for inclined tracks (50°) showing the distortion and the modulation effects. The horizontal scale is about 60 ns/div.

central plane of the chamber, and a saturated velocity is sufficient to guarantee a linear response. But for very inclined tracks, the shortest trajectory corresponds to electrons drifting along one cathode plane and then down to the anode, following the field lines. These
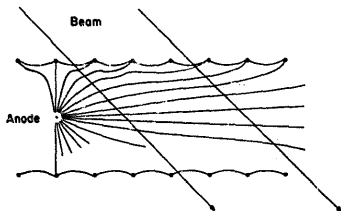

Fig. 17. Schema of the field lines in a drift chamber, showing the origin of the distortion and of the modulation that appears in the time spectrum (fig. 16) for large-angle tracks.
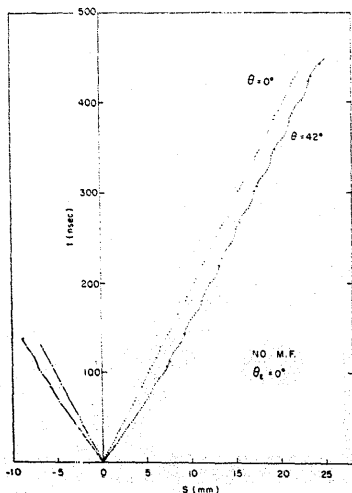
field lines are radial around the anode wire, and then more or less parallel to the chamber plane; but very close to the cathodes, poles of potential, they are slightly deformed by new field lines that begin on the cathode wires themselves. The effect is schematically shown in fig. 17; a complete analytic calculation of the field and of the distortions of drift time can be found in a report by Bourgeois and Dufey[18]). From inspection of the figure, one can easily understand how inclined tracks crossing the chamber close to the drift wire have a higher apparent density (then appearing as a peak in the time spectrum), and also how electrons released in the cathode planes region close to a peak or a valley of the field lines are modulated in their time of arrival at the anode. The effect is spectacular on the time spectrum, but it amounts to a small perturbation of the space–time correlation, where only the integral of the drift velocity appears. In the integral spectrum of fig. 16 the modulation is not visible at all, while it can be detected in a precise scanning; it accounts for less than $\pm 50\ \mu m$ oscillations around the central value (fig. 18).

Fig. 18. Space–time relationship, as measured with the precise mechanical scanning, for perpendicular (0°) and large-angle (42°) tracks. The modulation effect is slightly exaggerated in the figure for better understanding; the maximum deviation of the measured points at 42° around the average is about $\pm 50\ \mu m$.
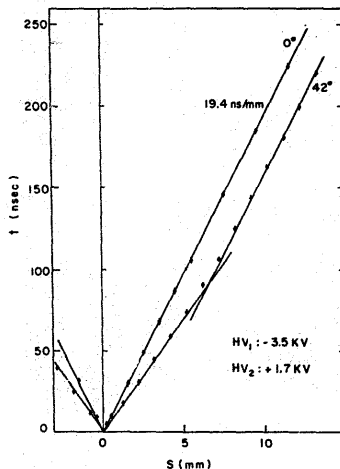

Fig. 19. Expanded view of the drift region close to the anode ($s = 0$) for 0° and 42° tracks. A two straight-lines fit to the large-angle data is shown, according to the simplified model described in the text.

We have verified the correctness of our explanation by building a special chamber with thin printed circuits replacing the cathode wires; with cathodes made of 1 mm printed strips, 1 mm apart, and with exactly the same HV distribution geometry as for the conventional chambers, no modulation was observed up to the biggest angles of incidence. We have not yet found, however, a suitable technique for building large chambers with thin printed electrodes; such a construction would have other advantages too, like better electrostatic screening of a gap from a neighbouring one.

We have computed that 1 mm spacing of cathode wires, instead of 2 mm, should reduce the modulation effect to a negligible one, and our designs of new chambers are presently modified in this sense.

Suitable algorithms are under study to take into account the angular distortion of linearity[18,19]. We would like to point out here how a very simple geometrical model represents a very good approximation to the data. Suppose that the trajectory of the closest electrons, drifting towards the anode, is radial on a direction perpendicular to the track from the anode up to the cathode plane, and then coincident with the cathode plane itself. One then gets

$$s = \frac{w}{\cos \theta}\, t, \qquad\qquad \text{for } 0 < t < \frac{g}{w \sin \theta}, \qquad (3)$$

$$s = wt + \left(\frac{g}{\sin \theta}\right)\left(\frac{1}{\cos \theta} - 1\right), \quad \text{for } t > \frac{g}{w \sin \theta}, \qquad (4)$$

where $2g$ is the gap (6 mm in our case), θ the angle of incidence of the track and w the (constant) drift velocity. The extent to which the two straight lines fit the measured data can be seen in fig. 19, which repeats in an expanded scale the first region of drift. It can be concluded, therefore, that although a knowledge of the angle of incidence is necessary to correct the angular distortion properly, the correction can be based on simple assumptions. A method to deduce the angle from the raw data, then correcting the distortion at the pattern recognition level, is under investigation[19].

4.5. ACCURACY

Using three chambers and the method delineated in section 3.4, we have measured the space accuracy of a drift chamber. In the computer display of fig. 20, the distribution of Δ, the deviation from a straight track given by eq. (2), is shown. The horizontal scale in the display is given in ns, and it should be recalled that the drift time is of about 20 ns/mm. The distribution has a nice Gaussian shape, with very few points, if any, on the tails, which are probably a consequence of large-angle δ rays or of non-correlated background. This confirms an additional advantage of working with small gaps (6 mm total in our case), as compared with the results obtained in MWPC where events with large clusters of hit wire are frequent[20]. The accuracy depends, of
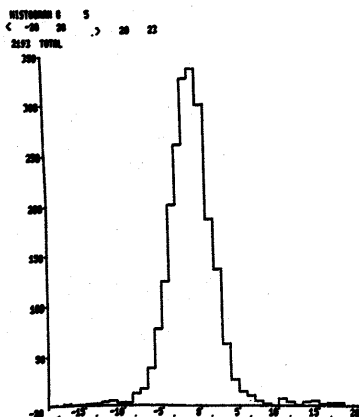

Fig. 20. Computer display of the dispersion in the three-chambers track reconstruction. $\Delta = \frac{1}{2}(t_1 + t_3) - t_2$, where t_1, t_2, t_3 are the times of drift in three equal-aligned chambers. The histogram is shown for $90 \leqslant t_2 \leqslant 110$ ns, corresponding to an average drift length of 5 mm. The horizontal scale is in ns.
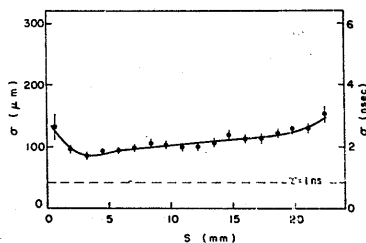

Fig. 21. Measured accuracy (standard deviation) for each chamber, as a function of the drift space, for perpendicular tracks. The electronic contribution to the dispersion, due to the finite binning width (1 ns), not deduced from the data, is also shown.

course, on the distance of drift, in principle according to a $\sqrt{s}$ law[10]. In our present measurement, however, we had a fixed electronic spread due to the 1 ns binning in the measurement of each asynchronous coordinate. In fig. 21 the measured standard deviation as a function of s is shown, for one chamber and $0°$ particles. The electronic contribution to the dispersion, not subtracted from the data, is also shown in the figure.

The measurement has been repeated for tracks inclined at $42°$, and the result is shown in fig. 22; we have plotted the accuracy in the plane of the chamber, whereas it should be realized that what plays a role in the reconstruction is the projected accuracy in a direction perpendicular to the tracks. The resulting accuracy is worse than for perpendicular tracks, and this is due to several factors:

i) The modulation effect, mentioned in section 4.4, scrambles the straight-line reconstruction since the "peaks" and "valleys" are randomly aligned in the three chambers at $42°$;

ii) The already-observed dependence of the pulse height and risetime on the angle spoils the data at large angles, since we work at fixed threshold;

iii) The statistical production of the primary electrons, generated along the particle trajectory at an average distance of about 300 μm in our gas, introduces a further dispersion on the minimum distance between the track and the anode.

The third effect does not play a big role for $0°$ tracks, apart from the region very close to the anode, where a deterioration of accuracy is in fact always observed for small s.

We have tried to improve the accuracy at large angles by measuring the time of the pulses not at threshold but at the peak, using modified photomultiplier peak stretchers*. If the worsening of accuracy had been mainly due to the statistics of ion pair formation and to the diffusion, we should have gained a factor $\sqrt{N}$, N being the number of primary electrons produced by the ionizing track. No improvement has been observed, suggesting that other effects (like amplifiers risetime, etc.) are predominant.

4.6. TIME RESOLUTION, MULTIPARTICLE RESOLUTION, AND RATE EFFECTS

The memory time of a chamber, having 50 mm wire spacing as in our case, is about 500 ns in our gas mixture. The time resolution is however much better; as it appears from figs. 21 and 22, between 2 and 4 ns (standard deviation). Of course, to make use of this

* Designed at CERN by H. Verweij and C. Engster.

very good intrinsic resolution, one needs several (at least three) chambers suitably staggered to detect a track. A method of electronic selection of good events, that is events satisfying an alignment condition in a coordinate plane, was already discussed in ref. 10 and is greatly simplified by the linearized space-time relationship, for not too large angles of incidence. In the general case, incoherent coordinates, that is points not satisfying the alignment condition, can be eliminated by software calculations. Clearly, however, the rather long memory of the chamber sets a practical limit on the total flux of particles (events and background) that can be tolerated in a given experiment.

We have studied in detail two other effects of high rates, i.e., the multiparticle resolution and the rate dependence of efficiency. When a track is amplified and detected on the anode wires, clearly a dead-time is produced by the system amplifier-discriminator. Operating at very low input impedances we have minimized the occupation time of the amplifier, defined as the time the input pulse exceed the threshold value; examples of the pulse width dependence on the angle of incidence were already presented in fig. 11. In that measurement, obtained in a small (20 cm × 20 cm) chamber, the occupation time varied between 30 ns (at $0°$) and 60 ns (at $60°$) corresponding to an electronic multitrack resolution on a wire between 1.5 and 3 mm. In the large chamber, however, we found another problem that could spoil the quoted resolution. The typical pulse detected on a very fast (risetime = 1.5 ns) $50\,\Omega$ preamplifier for minimum ionizing normal tracks is shown in fig. 23a. The main pulse, whose width does not exceed 20 ns, is followed by several smaller oscillations that would either retrigger a discriminator, or at
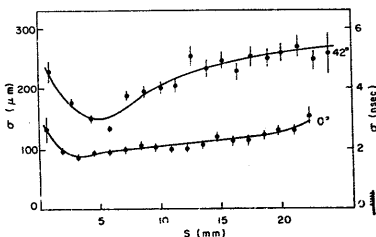

Fig. 22. Measured accuracy at $42°$ as compared to the $0°$ data. It should be noticed that the standard deviation has been computed in the plane of the chamber (direction of the coordinate s); for all applications, the important parameter is the accuracy projected on the normal to the tracks, $\sigma_\perp = \sigma \cos{(42°)}$.

least modify the time resolution of a close track. The effect is due to the bad matching between the frequency-dependent impedance of the anode wire and the amplifier that produces damped oscillations on the capacitive load. Introducing a damping resistor in series with the amplifier, we could eliminate the oscillations, but of course the trailing edge of the pulse got longer (fig. 23b). We are currently working on the problem of optimizing the load for the best multitrack resolution. One possibility is to differentiate slightly the signal at the input of the amplifier; this can safely be done since there are no positive associated pulses on the wire (as happens in MWPC, due to mutual induction between adjacent wires).

The well-known space-charge limitation adds to the described purely electronic effect to limit the multitrack resolution. When the ionizing events rate in a proportional counter gets large enough, the positive ions produced in the avalanche amplification at the anode create an effective screening for the electric field that reduces significantly the gain. In other words, the efficiency begins to be rate-dependent. Previous work on MWPC [21]) has shown that in chambers with 1 mm wire spacing an inefficiency appears at the level of 10^6 particles per cm^2 s. In a drift chamber having 50 mm wire spacing, the limiting rate should then be about

Fig. 23. Expanded view of the pulse detected, on a minimum-ionizing-particles beam, by a fast 50 Ω input-impedance amplifier mounted on the large drift chamber (upper part). A ringing effect appears, due to the impedance mismatching, that was not visible in the pulses of fig. 11 (obtained in a small chamber). Introducing a 220 Ω dumping resistor in series with the anode wire, we could obtain the smoothed pulse shown in the lower part. Depending on the threshold value, the effect sets a limit to the possible multitrack resolution. Horizontal scale: 20 ns/div. vertical 20 μA/div.

$2 \times 10^4/cm^2$ s; it should be noticed, however, that the quoted measurement has been obtained, operating the MWPC in a condition of very high gas amplification, at a density of positive ions probably one order of magnitude larger than in a normal operation of our drift chambers. To measure the space-charge limit, since the intensity in the test beam was not high enough for a direct measurement, we proceeded as follows. During a normal efficiency run, as described in section 4.3, the local rate was artificially increased approaching a strong (10 mCi) radioactive β source; the counting rate of the chamber itself provided a monitor for the flux. No decrease of efficiency was observed up to the highest rate we could obtain, $2.2 \times 10^4/cm^2$ s, which is about the expected limit. However, due to the large surface of the chamber, already at this rate we had a serious electronics problem: the singles rate of a wire was exceeding 10^6/s and the anodic current 200 μA, thus reducing the effective voltage. The measurement will have to be repeated in a beam of higher flux density and small surface. From the measured dc current corresponding to the detected rate, we could roughly deduce the multiplication factor, or gain, of the drift chamber: about 10^5. This is about one order of magnitude smaller than in conventional MWPC operating with the magic gas [13]) as used in ref. 21. Therefore we expect to gain about one order of magnitude in the maximum rate, due to the reduced positive-ion density [22]); this would bring the operational limit of the drift chambers to a flux of about 2×10^5 per cm^2 s.

5. Operation in magnetic fields

The main advantages of an AFDC: high accuracy and packaging density, are particularly important in vertex detectors operating in magnetic fields. The Lorentz force acting on the drifting electrons is however a perturbing factor, which would set a serious limitation on the wire spacing in the original design of an AFDC, the worst component being the field parallel to the anode wires. In this case, however, it was already shown [10]) how the equipotentials in the chambers can be tilted so as to compensate for the component of the magnetic force perpendicular to the cathode planes. Simple formulae exist to describe the motion of slow electrons in electric and magnetic fields: they are in general however applicable only in small electric fields (where the energy of the drifting electrons is mainly thermal [12,18,23]). We found that in the saturation mode, where we operate, those formulae were inadequate, and in the following only experimentally measured data are presented. A systematic study of drift velocity and drift angle in various gases and conditions has now
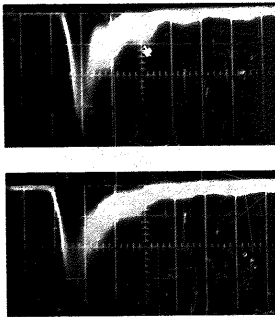
started in our group, with the hope of finding a gas mixture where the effect of the magnetic field is minimum; not necessarily, however, will such a gas satisfy the other requirements for proper operation. As an example, it was shown in ref. 10 that a larger percentage of isobutane reduces the lateral displacement
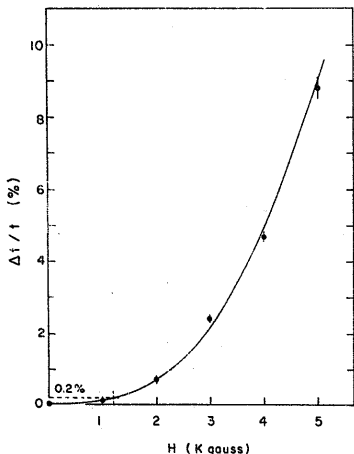

Fig. 24. Variation in the time of drift, due to a component of magnetic field parallel to the anode wires measured over 20 mm of drift space. To obtain a 50 μm stability over the maximum drift space, fields higher than 1.2 kG cannot be tolerated unless an appropriate correction to the data is applied.

due to magnetic fields, but the drift velocity was not saturated.

5.1. EFFECT OF SMALL MAGNETIC FIELDS

It is rather common in forward spectrometers that some chambers have to be operated in the leakage field of bending magnets. Due to the large variability of these fields, a compensation method, like the one mentioned in the introduction, would be very hard to realize, if not impossible, We have then measured in a standard AFDC connected for operation without magnetic fields, the perturbation generated by a small component of field parallel to the wires. The measurement was done installing three drift chambers in a magnet, and measuring the drift time for a given drift space as a function of H. The result is presented in

Fig. 25. Time spectra for a perpendicular beam obtained in a standard drift chamber at several values of the external magnetic field (parallel to the wires). The flat, rectangular-shaped spectrum refers to the measurement without magnetic field; at 5 kG, a slightly longer spectrum is obtained, due to the increased angle of drift of the electrons (see also fig. 24), but one still has full efficiency over 25 mm of drift. At 10 and 15 kG instead, the efficient region shrinks to about 15 and 10 mm, respectively. Horizontal scale: 80 ns/div.
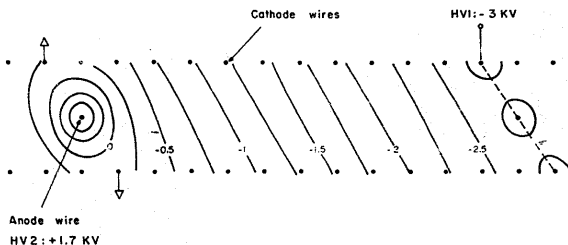

Fig. 26. Modification of the voltage distribution on the cathodes that permit the obtaining of inclined equipotentials to allow proper operation of a drift chamber in strong magnetic fields. The angle set in the figure (about 32°) is adopted for operation at 10 kG, the magnetic field being parallel to the wires.
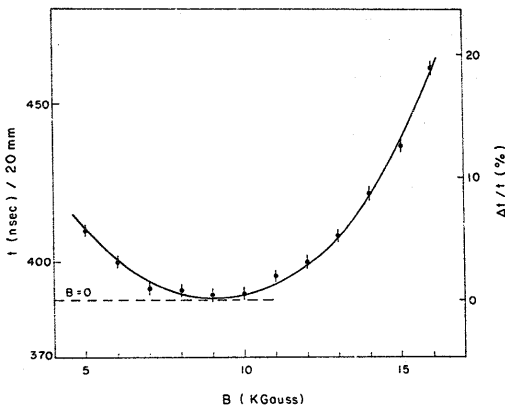
Fig. 27. Variation of the time of drift, measured over 20 mm, as a function of the magnetic field H for a fixed tilt angle of the electric field (as in fig. 26). The drift time at the minimum corresponds to the value of the drift velocity as measured at $H = 0$ (fig. 15). This proves that, at the high value of electric fields we are working on, the effect of the magnetic field is purely to bend the drifting-electrons' trajectory.

fig. 24, properly corrected for the bending of the beam traversing the three chambers, two of which were used for collimation as described in section 3.3. The curve reads as follows: if a maximum error of 50 μm can be allowed due to the (unknown) perturbation, $\Delta t / t$ should not, for the maximum drift space (25 mm), exceed 2×10^{-3}, i.e., an external component of the magnetic field as high as 1.3 kG can be tolerated. For higher values of the field, a correction is of course always possible based on the curve in fig. 24 and a knowledge of the local value of H. Notice that for 50 mm spacing, we had full efficiency of detection up to about 6 kG. The effect of an increasing magnetic field can be seen in the time spectra of fig. 25: when the field is zero, the normal square flat distribution is obtained. At 5 kG, the efficiency is still full over the drift space, but the time distribution is longer due to the bending of the trajectory of the drifting electrons; at 10 and 15 kG, however, the efficient region is reduced to about 14 and 9 mm with a strong deformation of the time distribution.

5.2. OPERATION IN STRONG MAGNETIC FIELDS

We have, for the time being, verified only the effect on the drifting electrons of the worst component of the field, i.e. the one parallel to the wires of the chamber that tends to sweep the electrons away from the medium plane. Modifying in a simple way the drift-voltage distribution, we were able to operate the chambers with the equipotentials in the drift region tilted by the amount required to compensate for the lateral deflection of the Lorentz force (fig. 26). For technical reasons, it was not possible yet to measure, as a function of the magnetic field, the tilt angle necessary to obtain proper drifting [this measurement is being done using a special chamber[11]]. Instead, at a fixed tilt angle, we have measured the drift time on a fixed length as a function of the vertical component of the magnetic field. The result is shown in fig. 27, for an average tilting of the electric field, θ_E, of 32°; the curve is a parabolic fit to the data. The minimum of the curve, at 9.5 kG, corresponds within the measurement errors to the value of the drift time in the absence of field (see section 4.4). In other words, we infer that for magnetic fields in the tesla region, the drift velocity in our saturated mode remains constant and equal to its value at $H = 0$, but the electrons drift along a trajectory making an angle (32° at 9.5 kG) with the electric-field equipotentials. Varying the magnetic field, then, a purely angular effect appears. This is better proved by figs. 28 and 29, where the space–time relationships for the operation at 10 and 12 kG are shown for perpen-

dicular tracks and constant θ_E as well as the corresponding efficiencies. The correlation is linear within the errors, with a slope increasing with the field value. From fig. 27, we can deduce the maximum variation around the optimum field, 9.5 kG, that can be tolerated to maintain a maximum 50 μm systematic error: about ±800 G. For larger variations, and in the region where the space–time relation remains linear (about ±3 kG around the minimum) the data have to be corrected using the measured distortion.

In fig. 28 the space–time relationship and the efficiency for inclined tracks is also shown; the distortion is similar to the one we have measured in the absence of magnetic fields, and the same considerations of section 4.4 apply. Due to the inclination of the equipotentials, one may have feared a different behaviour for tracks inclined in the same direction as the field (positive θ) or opposite to it (negative θ): this is not so, as shown in the figure where the measurements at

$\theta = +42°$ and $\theta = -42°$ overlap. For purely geometrical reasons, however, as can be easily understood by looking at fig. 26, the efficiency region is wider for the negative incidence (right-hand curve in fig. 28), while it coincides with the efficiency at $\theta = 0$ for positive θ.

For a comparison of performance, we have shown in fig. 30 similar results, for perpendicular tracks, obtained before we could run in full saturation. Not only is the relationship very unlinear, but also the dependence on magnetic field is much larger.

With the method described in section 3.4, but taking into account the bending of the beam, we have measured the accuracy of the chambers in the field. The results are shown in fig. 31 for perpendicular and inclined tracks. The accuracy is slightly worse than before, but many factors could contribute to the increase of the reconstruction errors in this case, as for example the large momentum bite of the beam, ±2%, not corrected in the reconstruction. It is known indeed that diffusion in strong magnetic fields, if anything, should decrease[23]).

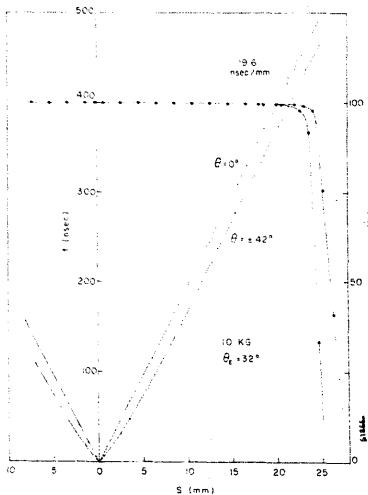No other relevant effects have been observed on the

Fig. 28. Space–time relationship at 10 kG, for perpendicular (slope 19.6 ns/mm) and inclined tracks. The efficiency plateau is also shown for $\theta = 0°$ (left-hand curve) and for $\theta = -42°$ (right-hand curve). The negative sign of θ refers to a direction of the beam opposite to the average direction of the electric field equipotentials (inclined by $\theta_E = +32°$). The chamber used in this measurement has 48 mm wire spacing.
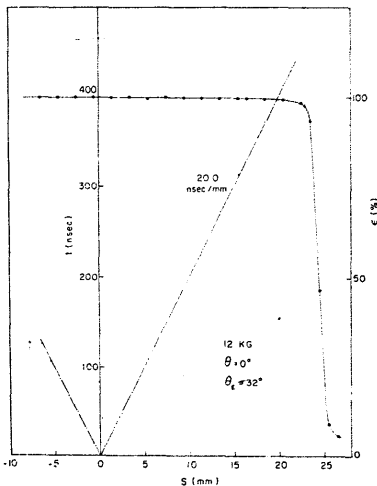

Fig. 29. Space–time relationship in the same chamber as for fig. 28, at 12 kG showing that linearity is maintained with a slightly different slope (20.0 ns/mm).

general operational parameters of the chambers due to the large magnetic fields. We can therefore conclude that drift chambers can be operated with full efficiency, good accuracy and linear response, in large and very large magnetic fields, provided the field strength does not change by more than $\pm 30\%$ along a given wire. To maintain the accuracy at the 100 μm level, a knowledge
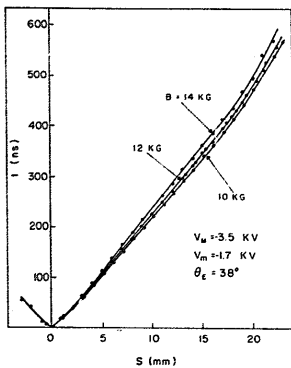

Fig. 30. Results measured in the same range of magnetic fields as in the previous figures before complete saturation in the drift velocity could be obtained. The average electric field in the chamber was of about 600 V/cm in a configuration similar to the one described in ref. 10. A much stronger dependence on the magnetic field value is visible, as well as a non-linear response close to the anode and to the field wires.
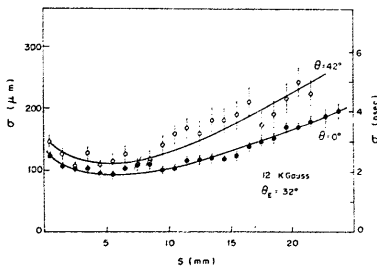

Fig. 31. Accuracies (standard deviation) as measured in 12 kG for perpendicular and inclined tracks. The results are very similar to the ones obtained without magnetic field, figs. 21 and 22.

of the field value within ± 800 G is required in order to correct the data properly.

6. The wire doublet scheme to resolve the right–left ambiguities

The right–left ambiguity is a very annoying characteristic of drift chambers, since in the general case it requires, to be eliminated, doubling of the measurement planes. It has been already mentioned that, to have good efficiency of reconstruction for multitrack large-angle events, not less than 6 coordinates per chamber are required[19]; only for simple, perpendicular, low multiplicity events can the number be reduced[9]. We have therefore tried to see if the ambiguity could be solved by a suitable construction of the chamber. It was already observed by some of us[24]) that, if two sense wires are mounted side by side and very close in a proportional chamber, discrimination on the amplitude of the induced pulses on the cathodes allowed right–left separation. Following this idea, we have replaced in the large (50 cm × 50 cm) drift chamber one normal-sense wire plane, with a plane having wire doublets. The wires in each couple are standard 20 μm wires, with the centres at 100 μm from each other, and are electrically insulated with independent output. The small distance was of course necessary to keep the remaining ambiguous region (half the wire spacing) below the 50 μm level. Due to the closeness of the wires in the couple, a strong electrostatic force repels each wire from the other; to a first order, the maximum sagitta of the deformed system can be given by:

$$\Delta y = Q^2 l^2 / (8\pi\varepsilon_0 Ty), \tag{5}$$

where Q is the charge of each wire, T the mechanical tension, y the distance between the wires and l their length.

Inserting in eq. (5) our typical parameters, i.e., $T = 50$ g (0.49 Newton), $Q = 12$ nC/m and $y = 10^{-4}$ m, one can compute that a mechanical link between the wires of the couple every 50 mm is necessary to gua-
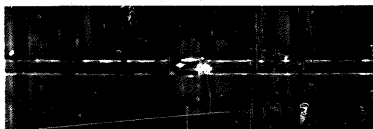

Fig. 32. Microscope picture of the link realized between two thin anode wires by a drop of epoxy. The distance between the wires in the couple is 100 μm, and the size of the drop about 120 μm × 200 μm.

rantee a maximum sagitta below 30 μm for each wire. The picture in fig. 32 shows how the link was realized. depositing a small droplet of epoxy on the couple. We have developed a simple technique to deposit properly the droplets on the required position; in the quoted chamber, 100 links have been realized (a drop every 50 mm, on ten couples) without failures; the longitudinal size of the drop, which can be evaluated in fig. 32 by comparison with the 100 μm wire spacing, varied between 100 μm and 400 μm in the worst case.

In fig. 33 the maximum separation between wires, as measured in the centre of the separation between two drops, is shown as a function of the anodic voltage; the full curve represents the computed value as from

eq. (5). The operational voltage of the chamber, with the wire couples, is about 2 kV, and there the maximum deviation is 60 μm.

The drift chamber with the quoted construction behaves very similarly to the standard one, only at a slightly higher anodic voltage (due to the reduced charge on each wire of the couple). The proof of a complete right-left separation can be seen in fig. 34, where a dual-trace scope triggered on the negative pulses of one wire of the couple shows on the adjacent wire (upper track) only positive induced signals. A more quantitative measurement was realized in the following way: the time spectrum of one wire in the couple was recorded, and then repeated (for the same incoming particle flux) requiring the adjacent wire to provide a negative pulse in coincidence. As can be seen in figs. 35a and b, even for large-angle tracks the number of coincidences is very small and can be entirely due to random counts. In other words, all tracks are only counted by one wire at a time; this is at first surprising for tracks traversing the region close to the wires at large angles. We think the effect is due to the combined action of the large positive induced signals, and to the space charge generated around the first counting wire.
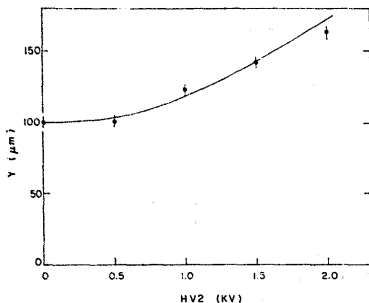

Fig. 33. Change in the average distance between the wires in a couple due to the electrostatic repulsion, as a function of the anodic potential. The distance is measured in the centre between two links, 50 mm apart. At the nominal working voltage, about 2 kV, the maximum deviation is of about 60 μm.
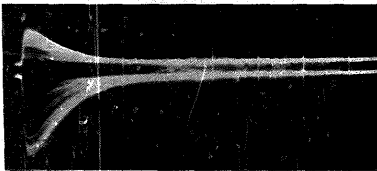

Fig. 34. Oscilloscope display showing the right-left separation, for a uniform irradiation of the chamber having wire couples. The scope is triggered on the lower negative trace, corresponding to the output from one wire of the couple, and in the upper trace the output of the second wire is shown. The appearance on it of only positive induced pulses shows that the same track is never counted by the two wires in coincidence.
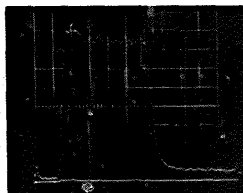

Fig. 35. Quantitative measurement of the right-left separation in a beam. In both pictures, the time spectrum of one wire in a couple is recorded (upper track) and then repeated requiring a coincidence from the other wire (lower track in each picture). The number of coincidences is below 1‰ even for large-angle tracks.

The measurements of linearity and accuracy have been repeated for the wire-doublet scheme, without any significant change as compared to the previously quoted results. One problem appeared, however, in the efficiency measurement: an integral efficiency not bigger than 97.5% has been found. The two possible sources of inefficiency, i.e., the region between the wires in the couple and the region around the glue drops, were then carefully investigated.

Fig. 36 shows the efficiency around the drops, as measured by a scanning along the direction of the wires; the inefficiency, localized around the drops, accounts for about 1% integral loss. We found that the remaining 1% loss was localized in the region close to the wire doublet, exceeding however their separation. This is shown in fig. 37, where the efficiency of each wire is measured in the cross-over region. The moderate steepness of the transition is of course almost entirely due to the scanning-beam collimation; still an inefficiency hole appears (broken curve) that would correspond to about 400 μm of 100% inefficiency. We could not yet find an explanation for this large effect, that accounts for the remaining 1% integral inefficiency. No inefficiency is measured between the two wires for inclined tracks (see fig. 38).

As a conclusion, we can say that at the price of a small, localized inefficiency the right–left ambiguity can be solved at the chamber level. The mechanical difficulty of constructing the wire couples is largely compensated by the reduction in the number of planes needed for an ambiguity-free reconstruction. Moreover, it appears[19]) that most of the computing time in the reconstruction programs comes from wrong couplings between points due to the right–left ambiguity. The wire-couple system has not yet been operated in magnetic fields; however, we do not expect particular problems.

7. Conclusions

The characteristics of drift chambers are in all respects optimum when they operate under conditions where the electric field saturates the drift velocity.
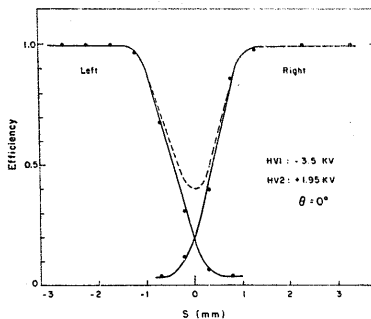

Fig. 37. Efficiency measurement in the region between the two wires of the couple for perpendicular tracks. There is a large localized inefficiency over about half a millimetre, that accounts for 1% integral loss.
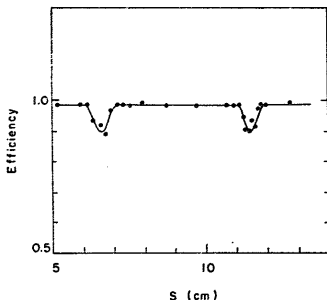

Fig. 36. Efficiency of the chamber for minimum-ionizing particles around the epoxy droplets; the links are 50 mm apart. The integral efficiency loss due to the links is about 1%.
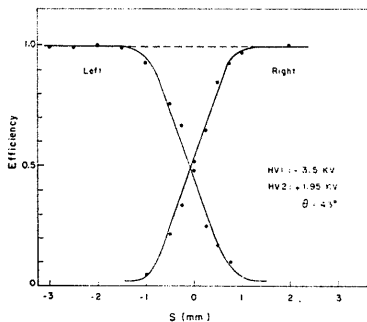

Fig. 38. The same measurement as in fig. 37, but for large-angle tracks: no inefficiency is detected. The complete details of the effect are still not well understood.

In summary, their main properties are the following:

i) an accuracy of about 100 μm is obtained over drift regions of 25 mm;

ii) the drift velocity does not change, within 1%, in magnetic fields of the order of 1 T;

iii) the response is linear, within the accuracy of 100μm, all over the drift space;

iv) the dependence of the drift velocity on gas compositions and temperature variations has been discussed and shown to be easily manageable;

v) there seems to be a simple way to solve the right–left ambiguity in a single plane with doublets of sense wires 100 μm apart, without degrading the accuracy over a sizeable region of the chambers.

The progress in the accuracy and reliability of drift chambers came together with some developments in the fields of their application.

Two-dimensional drift chambers can be built in a simpler way using a narrow delay line close to the sense wire and measuring the propagation time of the signal induced directly on the delay line[25]. This opens the way for many new applications of the drift chambers. Simple cylindrical chambers in solenoidal magnetic fields can thus be envisaged. For X-ray imaging, interesting applications can be found whenever the zero time can be given from an exterior source, like for instance with the synchroton radiation from electron storage rings where the X-ray pulses may be as narrow as 1 ns.

Drift chambers have also been shown to operate satisfactorily at pressures as low as 20 torr[26]. This opens up a wide range of applications in low-energy nuclear physics.

We wish finally to emphasize that the 100 μm accuracy limit is introduced mainly by our measuring methods. There is a wide open field of research in the direction of a serious improvement of this accuracy which may have a growing importance in high-energy physics.

We wish to thank H. Verweij and C. Engster of the electronics group of the NP Division of CERN for their support.

The skill of A. Dalluge and C. Jeanrenaud in the mechanical construction of the chambers has been essential for the realization of the measurements described.

References

1) G. Charpak, R. Bouclier, T. Bressani, J. Favier and Č. Zupan-čič, Nucl. Instr. and Meth. **62** (1968) 235.

2) G. Charpak, Ann. Rev. Nucl. Sci. **20** (1970) 195.

3) R. Bouclier, G. Charpak, E. Chesi, L. Dumps, H. G. Fischer H. J. Hilke, P. G. Innocenti, G. Maurin, A. Minten, L. Naumann, F. Piuz, J. C. Santiard and O. Ullaland, Nucl. Instr. and Meth. **115** (1974) 235.

4) G. Charpak, J. Phys. (France) **30** no. 5-6 (1969) C2-86.

5) T. Bressani, G. Charpak, D. Rahm and Č. Zupančič, Track localization by means of a drift chamber, Proc. Int. Seminar on *Filmless spark and streamer chambers*, Dubna 1969 (JINR, Dubna, 1969), p. 275.

6) R. Chaminade, J. C. Duchazeaubeneix, C. Laspalles and J. Saudinos, Nucl. Instr. and Meth. **111** (1973) 77.

7) A. H. Walenta, J. Heintze and B. Schürlein, Nucl. Instr. and Meth. **92** (1971) 373.

8) A. H. Walenta, A System of large drift chambers, Contr. to the 16th Int. Conf. on *High-energy physics*, Chicago-Batavia, 1972.

9) D. C. Cheng, W. A. Kozanecki, R. L. Piccioni, C. Rubbia, L. R. Sulak, H. J. Weedon and J. Wittaker, Nucl. Instr. and Meth. **117** (1974) 157.

10) G. Charpak, F. Sauli and W. Duinker, Nucl. Instr. and Meth. **106** (1973) 413.

11) M. Atkinson, A. Breskin, G. Charpak, F. Sauli and G. Schultz, Systematic measurements of drift velocities and angles in different gas mixtures and magnetic fields, to be published.

12) V. Palladino and B. Sadoulet, Application of the classical theory of electrons in gases to multiwire proportional and drift chambers, to be published.

13) G. Charpak, G. Fischer, A. Minten, L. Neumann, F. Sauli, G. Flügge, Ch. Gottfried and R. Tirler, Nucl. Instr. and Meth. **97** (1971) 377.

14) E. Schüller, A two-clock sensing system: a new time-to-digital converter, CERN-NP Intern. Rep. 73-15 (1973).

15) H. Verweij, Some remarks on electronics for drift chambers, Proc. Int. Conf. on *Instrumentation for high energy physics*, Frascati, 1973 (Lab. Naz. CNEN, Frascati, 1973) p. 616.

16) F. Sauli, Comments on some proposed schemes for drift chambers electronics, CERN-NP Intern. Rep. 73-12 (1973).

17) C. Rubbia, The time stretcher, a device to measure the time of electron drift in proportional chambers, CERN-NP Intern. Rep. 73-1 (1973).

18) F. Bourgeois et J. P. Dufey, Programmes de simulation des chambres à drift en champ magnétique, CERN-NP Intern. Rep. 73-11 (1973).

19) D. Townsend and N. Ford, Track recognition for drift chambers, CERN/DD report, to be published.

20) See, for example, M. Cavalli-Sforza, M. G. Goggi, W. W. Ash, D. C. Cheng, D. G. Coyne and G. K. O'Neill, Nucl. Instr. and Meth. **113** (1973) 87.

21) B. Sadoulet and B. Makowski, Space charge effects in multi-wire proportional counters, CERN/D-Ph 2 PHYS. 73-3, submitted to Nucl. Instr. and Meth.

22) L. Cohen, C. Grunberg and J. de Devechat, Nucl. Instr. and Meth. **103** (1972) 125.

23) J. Townsend, *Electrons in gases* (Hutchinson's Scientific Publications, London).

24) G. Charpak and F. Sauli, Nucl. Instr. and Meth. **107** (1973) 371.

25) A. Breskin, G. Charpak, F. Sauli and J. C. Santiard, Nucl. Instr. and Meth. **119** (1974) 1.

26) A. Breskin, G. Charpak and F. Sauli, Nucl. Instr. and Meth. **119** (1974) 7.